Acta Mechanica Sinica (2012) 28(4):1022–1029
DOI 10.1007/s10409-012-0116-5

RESEARCH PAPER

The study of sound wave propagation in rarefied gases using unified gas-kinetic scheme

Rui-Jie Wang · Kun Xu

Received: 27 April 2012 / Accepted: 30 April 2012

Abstract Sound wave propagation in rarefied monatomic gases is simulated using a newly developed unified gas-kinetic scheme (UGKS). The numerical calculations are carried out for a wide range of wave oscillating frequencies. The corresponding rarefaction parameter is defined as the ratio of sound wave frequency to the intermolecular particle collision frequency. The simulation covers the flow regime from the continuum to free molecule one. The treatment of the oscillating wall boundary condition and the methods for evaluating the absorption coefficient and sound wave speed are presented in detail. The simulation results from the UGKS are compared to the Navier–Stokes solutions, the direct simulation Monte Carlo (DSMC) simulation, and experimental measurements. Good agreement with the experimental data has been obtained in the whole flow regimes for the corresponding Knudsen number from 0.08 to 32. The current study clearly demonstrates the capability of the UGKS method in capturing the sound wave propagation and its usefulness for the rarefied flow study.

Keywords Unified gas-kinetic scheme · Sound wave propagation · Non-equilibrium flows

1 Introduction

At a sufficient small Knudsen number, the sound propagation in gas can be adequately described by the Navier–Stokes equations. However, as Knudsen number increases to the transition regime, the sound wave parameters, i.e., phase speed and attenuation coefficient, are known to deviate from the classical prediction. Most existing hydrodynamic equations fail to describe the ultrasound propagation. This is not surprising because the scale for the hydrodynamic equations is in the diffusive scale due to the spatial and temporal variation of local equilibrium states, and this modeling scale is much larger than the kinetic scale which is in the particle mean free path and particle collision time. At high frequency, the period of the sound wave propagation can easily come to the kinetic scale, which is comparable with the particle collision time. In order to investigate the high frequency sound wave propagation, many researchers turned attention to the kinetic equations by means of theories based on the expansion of Boltzmann equation. Wang Chang and Uhlenbeck [1] utilized the Super-Burnett equations, which were then extended by Pekeris et al. [2] up to 483 moments. However, the success of these theories can not be extended to high Knudsen number flow regime. A remarkable success that performs well for a wide range of Knudsen numbers is the work of Sirovich and Thurber [3], and also Buckner and Ferziger [4]. Sirvoich and Thurber used Gross-Jackson model and analyzed the dispersion relation, where Buckner and Ferziger solved the half-space problem by means of elementary solutions, with diffusely-reflecting boundary. Besides the Gross-Jackson model, another popular kinetic model used for the study of sound wave is the BGK model. Thomas and Siewert [5] and Loyalka and Cheng [6] adopted the BGK model and solved the problem in half-space together with diffusely-reflecting boundary. Their results agreed with each other. As reported in Ref. [7], they obtained better agreement with experimental measurements than the BGK results of Sirovich and Thurber [3] and those of Buckner and Ferziger [4]. Another successful method in simulating ultrasound wave propagation is the direct simulation Monte Carlo (DSMC) method [7], and the DSMC method is basically solving the Boltzmann equation as well.

In this paper, a newly developed unified gas-kinetic scheme (UGKS) [8–10] will be used to perform numerical

R.-J. Wang
Nano Science and Technology Program
Hong Kong University of Science and Technology
Clear Water Bay, Kowloon, Hong Kong, China

K. Xu (✉)
Mathematics Department
Hong Kong University of Science and Technology
Clear Water Bay, Kowloon, Hong Kong, China
e-mail: makxu@ust.hk

simulation of sound propagation in monatomic gases for the whole Knudsen regime with hard-sphere molecule. Comparison is made with experimental results of Greenspan [11] and Meyer and Sessler [12], and the DSMC results of Hadjiconstantinou and Garcia [7]. Good agreement is found between our results and the experimental measurements. This is another clear case which demonstrates the capability of the UGKS method in capturing the non-equilibrium phenomenon.

2 Unified gas-kinetic scheme

The UGKS is a scheme based on the gas-kinetic BGK and Shakhov model in simulating flows in the whole Knudsen regimes [8–10]. It is a multi-scale method which updates both macroscopic conservative flow variables and microscopic gas distribution function. The novelty of the approach is the coupled treatment of particle transport and collision process in the evaluation of interface fluxes for the update of both macroscopic variables and microscopic distribution function. The integral solution used for the flux evaluation covers the whole regime from the kinetic to the hydrodynamic ones, and the specific solution used locally at a cell interface depends on the ratio of computational time step to the particle collision time.

For a unified scheme to simulate flow in all Knudsen regimes, it is necessary to capture both hydrodynamic and kinetic scale gas evolution. In the hydrodynamic scale, the flow physics is mainly determined by the pressure waves, and in the kinetic scale the individual particle transport plays an important role in the description of non-equilibrium state. In the transition regime, both wave and particle effect will take place and this is also the main difficulty to capture the transition flow. The most widely used approach for the whole flow regime simulation is the hybrid method, where the underlying philosophy of the hybrid approach is that there is a region where both hydrodynamic and kinetic descriptions are valid. This hope may not be true because in the transition regime we can not set up a valid physical principle for the conversion of wave and particle descriptions. In principle, it is generally agreed that the Boltzmann equation covers the flow regime from the free molecule to the equilibrium Euler solutions, and a unified scheme based on the Boltzmann equation can be developed. However, if we think of the modeling process in the construction of the Boltzmann equation, we will realize that the development of a unified scheme based on the full Boltzmann equation can be hardly achieved. The modeling scale of the Boltzmann equation is in the particle mean free path and particle collision time scale. In order to solve the Boltzmann equation truthfully, the mesh size used must be compatible with the particle mean free path and the numerical time step is on the order of particle collision time. This constraint on the time step and cell size is fully implemented in the DSMC method which is supposed to be a method for solving the Boltzmann equation in the limiting case. So, based on the original Boltzmann equation, it will be hard to develop a unified scheme which is efficient in the continuum flow regime. In the continuum flow region, one cell size can be on the order of thousands of particle mean free path, such as the case of high Reynolds number boundary layer with a few grid points, and the Boltzmann equation is not modeled on the numerical cell size scale in its collision process. Therefore, the modeling scale of the collision term in the Boltzmann equation prevents the development of a unified scheme in the continuum regime. Actually, it has the similar reason why we can not use molecular dynamics to solve the flow problem in the continuum regime, because the scale of molecular dynamic modeling is even smaller. The modeling scale of the Boltzmann equation is not large enough for the capturing continuum flow behavior. Certainly, we can expand the distribution function around the equilibrium state in the continuum regime and substitute it back into the Boltzmann equation. But this linearization process may introduce accuracy problem in the transition regime, especially in the cases with large temperature variation.

In the multiscale modeling aspect, the BGK-type equation in some aspect may provide a better model to cover the whole flow regime. The BGK equation is a gas-kinetic relaxation model, which has no an explicit scale constraint in its modeling. The merit of the BGK model is the explicit appearance of the equilibrium state, and the drifting of the equilibrium state will directly recover the hydrodynamic flow physics of the Navier–Stokes solution on a dissipative scale, which is much larger than the kinetic one.

The unified scheme is not a purely numerical partial differential equation (PDE) solver of the kinetic BGK model. It is a PDE-based modeling method, where the time dependent integral solution of the PDE is used for the evaluation of a time dependent gas distribution function at a cell interface. The valid time scale of this integral solution can go theoretically far beyond the particle collision time. This time scale can be related to the spatial resolution, such as the cell size, through the CFL condition. Due to the different scales of the numerical cell size in comparison with the particle mean free path in a numerical scheme, the flow transport passing through a cell interface can recover the flow physics in different flow regimes. If the mesh size is smaller than the mean free path, the free molecule transport, or the upwind approach, can be recovered from the integral solution. When the cell size is much larger than the particle mean free path, the intensive particle collision in the transport process will converge the integral solution to the exact Navier–Stokes gas distribution function for the description of continuum flow. Therefore, the integral solution of the kinetic model covers both hydrodynamic and kinetic scale flow physics, and there is no hybrid or switch function needed to get these limiting cases. In summary, the unified scheme is a finite volume method, which updates both conservative flow variables and the gas distribution function. The evaluation of the interface flux is based on the integral solution of the kinetic model,

the so-called the PDE evolution solution-based modeling. The detail formulation of the unified scheme can be found in Refs. [8–10].

3 Sound propagation simulation method

Figure 1 shows the schematic of the simulation geometry. The monatomic argon gas is enclosed between two walls separated by a distance L. The left wall is the transducer which is imposed by a periodical velocity $U(t) = U_0 \cos \omega t$ and the particles are diffusely reflected from the wall. On the other hand, the right wall is a resting receiver and is assumed to have a specular boundary condition, which leads to total reflection of the propagating waves. The flow field is assumed to be one-dimensional. There are two relevant Knudsen numbers Kn for this problem, one is defined as the ratio of mean free path λ to the domain length L, and the other is the ratio of wave frequency ω to particle collision frequency $1/\tau$,

$$Kn_L = \frac{\lambda}{L}, \quad Kn_\omega = \omega\tau,$$

where λ is the particle mean free path, L is the domain length, ω is the angular frequency of wave, and τ is the particle collision time.

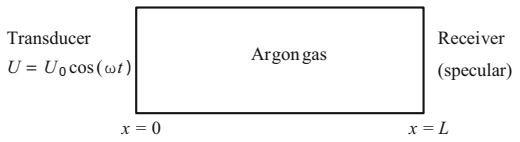

Fig. 1 Schematic of the simulation geometry

3.1 Dimensionless variables

The dimensionless quantities are defined through the reference state denoted by $\rho_\infty, T_\infty, P_\infty$ etc.,

$$\hat{t} = \frac{t}{\tau_\infty}, \ \hat{u} = \frac{u}{C_\infty}, \ \hat{x} = \frac{x}{\lambda_\infty},$$
$$\hat{\rho} = \frac{\rho}{\rho_\infty}, \ \hat{T} = \frac{T}{T_\infty}, \ \hat{P} = \frac{P}{\rho_\infty C_\infty^2},$$

where u is the particle velocity in x-direction. Here $C_\infty = \sqrt{R_0 T_0}$, $T_\infty = T_0/2$, $\lambda_\infty = \mu_0 \sqrt{R_0 T_0}/P_0$, $\tau_\infty = \tau_0$, $\rho_\infty = \rho_0$, and $T_0, \mu_0, P_0, \rho_0, \tau_0$ are corresponding flow parameters in the rest state. Here R_0 is the gas constant. The reference state is chosen for convenience.

For hard-sphere molecular, the particle mean free path is $\lambda_0 = 8\sqrt{2/\pi}/5\lambda_\infty$, and the two relevant Knudsen numbers are

$$Kn_L = \frac{\lambda_0}{L} = \frac{8}{5\hat{L}}\sqrt{\frac{2}{\pi}}, \quad Kn_\omega = \omega\tau_0 = \hat{\omega}. \tag{1}$$

The dimensionless form of classical sound speed at rest state is $\hat{c}_0 = \sqrt{\gamma R_0 T_0}/\sqrt{R_0 T_0} = \sqrt{\gamma}$. For monatomic gases, $\hat{c}_0 = \sqrt{5/3}$. All variables below are expressed in dimensionless form, and the hat is dropped for simplicity.

3.2 Boundary condition

In our simulation, the boundary treatment of the left wall is different from the Maxwellian reservoir method used by Hadjiconstantinou and Garcia in their DSMC simulation [7]. Following Loyalka and Cheng and others [6, 13], the maxwellian distribution at the wall is set to be

$$g_w = \rho\left(\frac{\lambda}{\pi}\right)^{3/2} \mathrm{e}^{-\lambda[(u-U_0\cos\omega t)^2+v^2+w^2]}, \ u > 0, \tag{2}$$

and the density at the thermal wall is determined by

$$\int_{t^n}^{t^{n+1}} \iiint_{u>0} (u - U_0 \cos\omega t) g_w \mathrm{d}u\mathrm{d}v\mathrm{d}w\mathrm{d}t + \int_{t^n}^{t^{n+1}} \iiint_{u<0} (u - U_0 \cos\omega t) f_{in} \mathrm{d}u\mathrm{d}v\mathrm{d}w\mathrm{d}t = 0, \tag{3}$$

where f_{in} is the distribution function of particles impinging on the wall. Then, the flux across the wall can be calculated as

$$\boldsymbol{F} = \begin{bmatrix} F_\rho \\ F_{\rho U} \\ F_{\rho E} \end{bmatrix} = \int_{t^n}^{t^{n+1}} \iiint_{u>0} u g_w \boldsymbol{\phi} \mathrm{d}u\mathrm{d}v\mathrm{d}w\mathrm{d}t + \int_{t^n}^{t^{n+1}} \iiint_{u<0} u f_{in} \boldsymbol{\phi} \mathrm{d}u\mathrm{d}v\mathrm{d}w\mathrm{d}t, \tag{4}$$

where $\boldsymbol{\phi} = [1, u, (u^2+v^2+w^2)/2]^{\mathrm{T}}$ is the moments for conservative variables. The effect of different boundary treatment on the solution will be discussed later.

3.3 Method for determining sound parameters

In the experiment, one measures the pressure signal at the receiver and assumes that the pressure is a single damped wave of the form

$$P(x,t) = A\exp[\mathrm{i}(\omega t - kx + \varphi) - mx], \tag{5}$$

where A is amplitude, ω is angular frequency, k is wave number, m is attenuation coefficient and φ is phase shift. Linear fits are performed in logarithm plots of amplitude and phase over a range of distances between the transducer and receiver in order to determine the parameters in the above equation.

In our simulation, the flow variables in the whole domain is obtained in each computation, which enables us to extract the sound parameters without changing the domain length. Similar to the method used by Hadjiconstantinou and Garcia [5], the wave can be expressed as

$$U = A(x)\cos\omega t + B(x)\sin\omega t, \tag{6}$$

and a least-square method is used to extract $A(x)$ and $B(x)$ from the numerical solution after the initial transients (approximately after 60 periods), which are given by

$$A(x_j) = \frac{\sum s^2 \sum vc - \sum sc \sum vs}{\sum c^2 \sum s^2 - (\sum sc)^2},$$

$$B(x_j) = \frac{\sum c^2 \sum vs - \sum sc \sum vc}{\sum c^2 \sum s^2 - (\sum sc)^2},$$

where

$$\begin{aligned}
\sum s^2 &= \sum_i \sin^2 \omega t_i, \\
\sum c^2 &= \sum_i \cos^2 \omega t_i, \\
\sum sc &= \sum_i \sin \omega t_i \cos \omega t_i, \\
\sum vs &= \sum_i U(x_j, t_i) \sin \omega t_i, \\
\sum vc &= \sum_i U(x_j, t_i) \cos \omega t_i,
\end{aligned}$$

with x_j being the x-coordinate of cell center and t_i being the time to do the sampling. Then the amplitude can be calculated by $\sqrt{A(x)^2 + B(x)^2}$. If we further express the wave propagating in the positive direction as

$$V_0 \exp[\mathrm{i}(\omega t - kx + \varphi) - mx],$$

and the reflected wave as

$$-V_0 \exp[\mathrm{i}(\omega t + k(x - 2L) + \varphi) + m(x - 2L)],$$

the superposition leads to

$$\begin{aligned}
U &= V_0 \exp(-mx) \cos(\omega t - kx + \varphi) \\
&\quad -V_0 \exp[m(x - 2L)] \cos[\omega t + k(x - 2L) + \varphi]. \qquad (7)
\end{aligned}$$

Combining Eq. (7) with Eq. (6) gives

$$\begin{aligned}
A(x) &= V_0 \exp(-mx) \cos(kx - \varphi) \\
&\quad -V_0 \exp[m(x - 2L)] \cos[k(x - 2L) + \varphi], \qquad (8)
\end{aligned}$$

and

$$\begin{aligned}
B(x) &= V_0 \exp(-mx) \sin(kx - \varphi) \\
&\quad +V_0 \exp[m(x - 2L)] \sin[k(x - 2L) + \varphi]. \qquad (9)
\end{aligned}$$

In the above formulas, V_0, φ, m, k are unknowns, and are obtained by parameter estimation using the Nelder-Mead simplex method, which is available in most mathematical softwares. The formula used by Hadjiconstantinou and Garcia is a little bit different from Eq. (7). They simplified the expression under the condition $L = (7/4)l$, where L is the domain length and l is the wavelength.

In low frequencies, the estimation of wave parameters are based on the amplitude

$$\begin{aligned}
&\sqrt{A(x)^2 + B(x)^2} \\
&\quad = V_0 \sqrt{4\mathrm{e}^{-2Lm}\{\cosh[2m(x - L)] - \cos[2k(L - x)]\}} \qquad (10)
\end{aligned}$$

However, in high frequencies, the reflected wave is very weak in comparison with incoming one and the amplitude approximately takes the following form $V_0 \exp(-mx)$. The information of phase speed is lost in the expression of the above amplitude, and the estimation of wave parameters for high frequency wave is directly based on both $A(x)$ and $B(x)$ in Eqs. (8) and (9). According to the analysis in Ref. [14], the wave is composed of several modes in low frequencies, instead of one mode described by Eq. (7). Within all transport modes, the so-called acoustic mode dominates the transport, and the other modes get damped quickly. By excluding the region near to the transducer, the fitted result using Eq. (10) is actually the acoustic mode in low frequencies (shown in next section). In high frequencies, however, the sound parameters show an increasing dependence on the location, which was observed in other numerical computations [5–7] and was analyzed in free-molecular limit [15]. Under this condition, Eqs. (5) and (7) are not applicable for high-frequency waves in the whole domain. Since all experimental measurements do not include the information about the region where the sound parameters are measured, we determine the numerical region for estimating wave parameters by gradually excluding the region near the transducer until a best fit for the rest of the domain is obtained.

3.4 Simulating cases

We have performed simulation for a wide range of frequencies from $\omega = 0.08$ to $\omega = 32$. Based on Eq. (1), the corresponding Knudsen number Kn_ω ranges from 0.08 to 32. The domain length L is chosen to be no more than a few wave lengths, which is approximately $L \approx (7/4)l$, where l is the wavelength. The wave frequencies and domain lengths are listed in Table 1. Based on Eq. (1), the Knudsen number Kn_L changes from 0.007 to 1.28.

Table 1 Sound wave frequencies and domain length

ω	0.08	0.10	0.20	0.25	0.40	1.00	2.00	2.50	3.20	4.00	5.00	8.00	16.00	32.00
L	175.00	140.00	70.00	58.00	38.00	16.00	8.50	7.00	6.00	5.50	4.50	3.55	2.00	1.00

In order to avoid nonlinear effect, such as shock formation, in the wave propagation, the requirement

$$Re = \frac{\rho_0 U_0 c_0}{\omega \mu_0} \ll 1,$$

should be met. By introducing the acoustic Reynolds number,

$$R = \frac{c_0^2 \rho_0}{\omega \mu_0} = \frac{\gamma}{\omega},$$

the requirement can be written as $U_0 \ll c_0/R$. For frequencies $\omega \leq 0.25$, we use $U_0 = 0.005$; for $0.4 \leq \omega \leq 2.5$, we use $U_0 = 0.01$; and for even higher frequencies, we use $U_0 = 0.02$. To capture the wave profile accurately, we use 140 cells in most cases, which is approximately 80 cells per wavelength. For $\omega = 8.0$, 70 cells are used. For extremely high frequencies $\omega = 16.0, 32.0$, only 35 cells are used. The time step is determined by the CFL condition, and it also satisfies the requirement,

$$\Delta t < \frac{\pi}{30\omega},$$

in order to accurately capture the time evolution of the wave profile.

4 Numerical results

The time to start sampling is determined by setting a monitor point, where the velocities at each moment of integer period, i.e., at time $t = n(2\pi/\omega)$ with $n = 1, 2, ...$, are recorded. When the changing of velocities becomes substantially small, we start the sampling. Figure 2 shows the velocity change at the monitor point for $\omega = 0.1$.

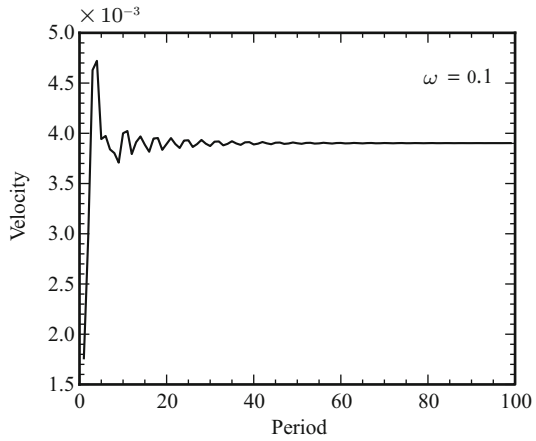

Fig. 2 Velocity change on every integer period at the monitor point for $\omega = 0.1$

To extract $A(x)$ and $B(x)$, we start sampling from 100 periods to 110 periods, with 100 time samples in each period. Figure 3 shows $A(x)$ and $B(x)$ for $\omega = 0.1$.

In low frequencies, the estimation of wave parameters is based on the amplitude definition of Eq. (10). Figure 4 shows the simulated and fitted amplitude at $\omega = 0.1$ from the UGKS simulation. In order to validate our result, the rescaled analytic solution of Regularized 13-moments (R13) equation [13] is also included for comparison. In order to have a real comparison with the R13 result, the same isothermal wall boundary condition as R13 is used in our simulation. Since $\omega = 0.1$ is a relative low frequency, the R13 result should be reliable even though it does not work properly for high frequency wave. The above comparison confirms that by excluding the region near to the transducer, the fitted amplitude using Eq. (10) recovers the acoustic mode.

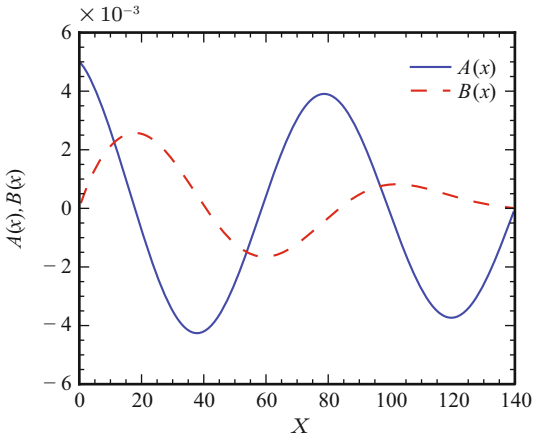

Fig. 3 $A(x)$ and $B(x)$ for $\omega = 0.1$

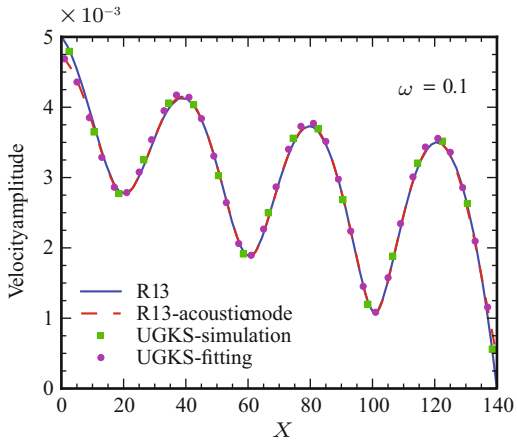

Fig. 4 Simulated and formula fitted amplitude for UGKS results and the theoretical solutions of R13 at $\omega = 0.1$

In high frequencies, the estimation of wave parameters are based on both $A(x)$ and $B(x)$ presented in Eqs. (8) and (9), and the region used for fitting is determined by gradually exclude the region near the transducer until a best fit for the rest domain is obtained. Figure 5 shows one of the fitted result of $A(x)$, $B(x)$ at $\omega = 5$ by matching the numerical solutions with the analytical ones in Eqs. (8) and (9) and the corresponding velocity amplitude.

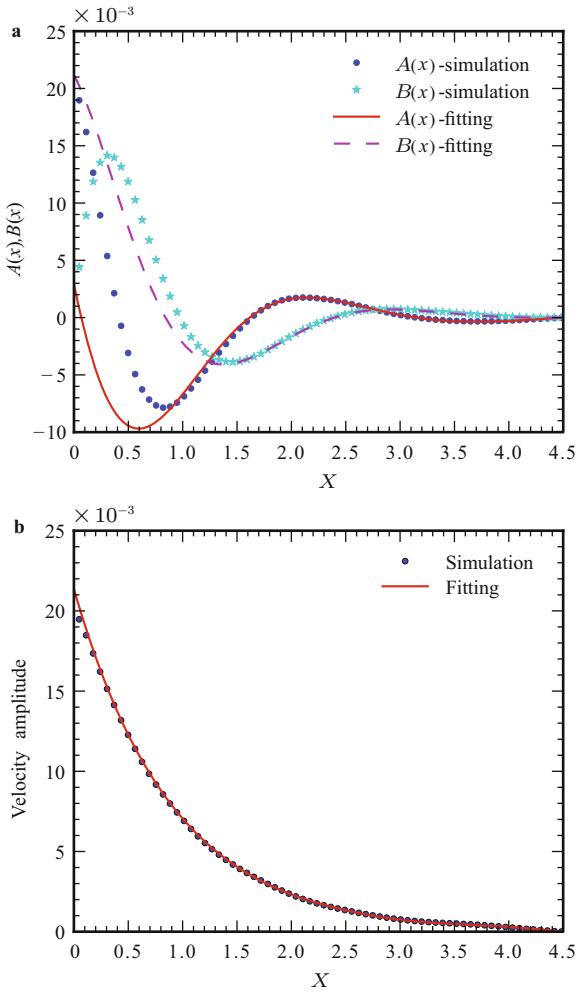

Fig. 5 Simulated and fitted results for $\omega = 5$

The location dependent behavior of the phase speed and attenuation coefficient in high frequencies can be observed by changing the region used for fitting. Figure 6 shows the fitted phase speed start from different locations $x_{\min}$ for $\omega = 5$. The fitted result in Fig. 5 is based on the sampling point starting from $x_{\min} \approx 1.54$. In the high frequency case, the point-wise definition of wave parameters used by Schotter [16], Garcia and Siewert [13], and Sharipov [15] may be another choice for their evaluation.

The final results of phase speed and attenuation coefficient are listed in Table 2. The comparison among the experiments, DSMC, Navier–Stokes solutions, and the UGKS results are presented in Figs. 7 and 8, respectively.

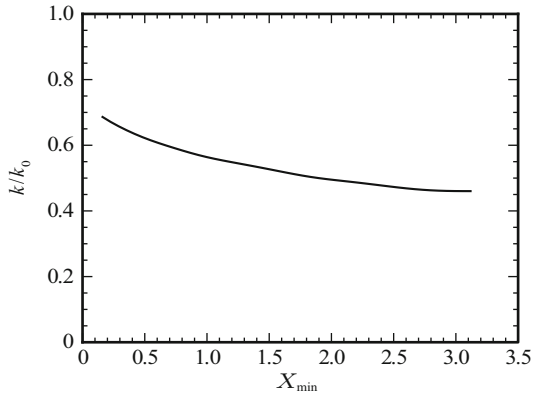

Fig. 6 Location dependent phase speed for $\omega = 5$

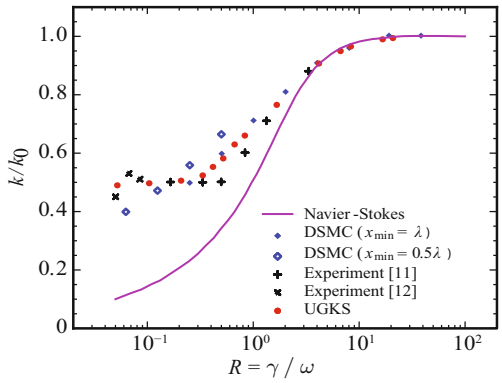

Fig. 7 Phase speed comparison at different frequencies among the results from UGKS, DSMC, experimental measurements, and Navier–Stokes equations

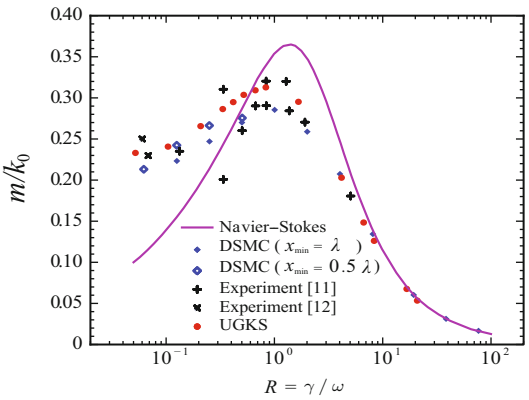

Fig. 8 Attenuation coefficient comparison at different frequencies among the results from UGKS, DSMC, experimental measurements, and Navier–Stokes equations

Table 2 Test results for wave speed and attenuation coefficient

ω	0.08	0.10	0.20	0.25	0.40	1.00	2.00	2.50	3.20	4.00	5.00	8.00	16.00	32.00
k	0.062	0.077	0.150	0.184	0.281	0.593	1.023	1.220	1.442	1.713	2.028	3.134	6.159	1.214
m	0.003	0.005	0.020	0.029	0.063	0.229	0.485	0.599	0.753	0.914	1.109	1.646	2.983	5.777

It is obvious that the UGKS results have a good agreement with the experimental data. Although the boundary treatment and numerical method used in our simulation are different from that in DSMC calculation, the main difference in the UGKS and the DSMC results does not come from them, but the region used for fitting the numerical solution by the formula. The DSMC simulation fixed the starting location for fitting at $x_{\min} = \lambda$ or $x_{\min} = 0.5\lambda$. If the same fitting location is used, it is expected to obtain similar results for both UGKS and DSMC methods. Figure 9 shows $A(x)$ and $B(x)$ for $R = 0.5$ ($\omega \approx 3.3$) using the UGKS and the DSMC data, with the same boundary condition (Maxwellian reservoir method). The results are almost the same from two different methods, and the estimated wave parameters only have a slightly difference from that obtained by the boundary treatment in Eqs. (2)–(4). Since $Kn_\omega = \omega \approx 3.3$ is a pretty large Knudsen number, the perfect match between UGKS and DSMC solution confirms the accuracy of the UGKS method in capturing non-equilibrium flow.

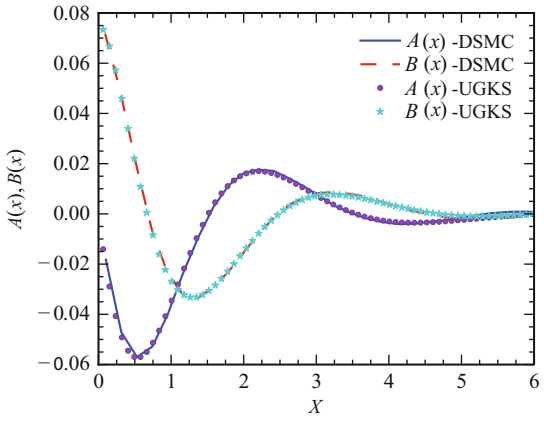

Fig. 9 Comparison of UGKS and DSMC results using the same boundary condition at $R = 0.5(\omega \approx 3.3)$

The UGKS results are also compared with the original experimental data presented by Greenspan [4] and Meyer [8] in Figs. 10 and 11. It can be seen that the current results have good agreement with the experimental data in general, especially in the continuum regime and free-molecular regime. In regime $2 \leqslant \omega \leqslant 4$, the phase speed have a slightly overshot. This overshot is also observed in other computations [4–7].

5 Discussion and conclusion

In this paper, the sound wave propagation in monatomic gases is simulated with hard-sphere molecule for the whole Knudsen regime, and the phase speed and attenuation coefficient are obtained. The good agreement between the UGKS results and the experimental data is another validation of the UGKS method in capturing the physical solutions for non-equilibrium flows.

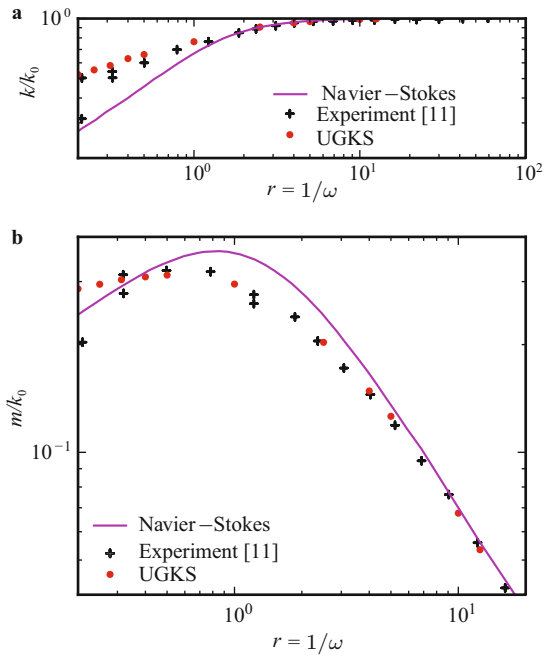

Fig. 10 Results comparison between UGKS results and experimental data of Greenspan [11]

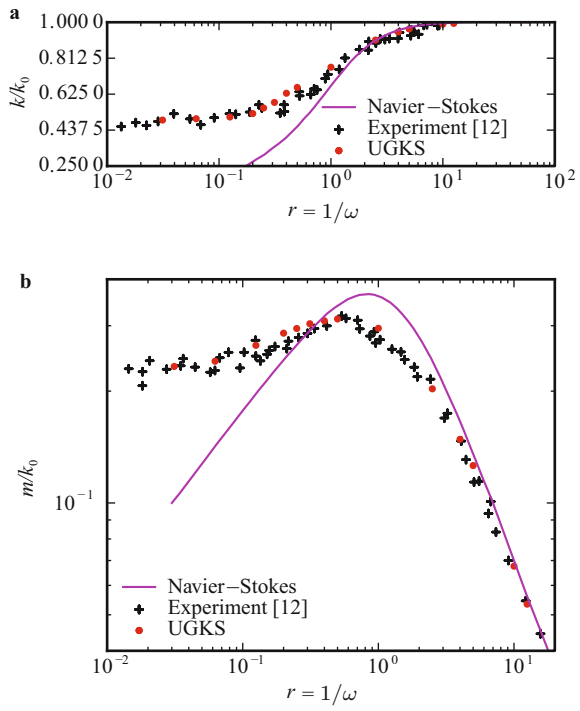

Fig. 11 Results comparison between UGKS results and experimental data of Meyer [12]

There are several differences between the UGKS and the DSMC method for the sound wave simulation. First, the boundary treatment of the transducer in our simulation is different with the Maxwellian reservoir method used by the DSMC method [5]. However, as shown in this paper, different boundary treatments only have marginal effect on

the evaluation of phase speed and attenuation coefficient. Second, the hard-sphere molecule is used in our simulation, which corresponds to $\mu \sim \sqrt{T}$. We can easily extend the UGKS method to simulate any viscosity law, such as the Sutherland's law. For the DSMC method, it is not too obvious to easily incorporate any general viscosity laws, besides the hard-sphere and variable hard-sphere models. By contrast, the viscosity coefficient in UGKS can be directly implemented through the determination of the local particle collision time. For the traditional BGK modeling and simulation, people usually used a constant particle collision time. However, for the UGKS method, the particle collision time is a time and space dependent function of flow variables. This needs to be emphasized for the UGKS method.

The wave propagation in high frequencies/high Knudsen number flow is quite different with the classical sound wave results. With the increasing dependence of phase speed and attenuation coefficient on the location for their evaluation, the wave behavior lost its classical form, and can not be described by Eqs. (5) and (7). A point-wise definition [13, 15, 16] of phase speed and attenuation coefficient is more appropriate in such a situation.

Acknowledgement The project was supported by Hong Kong Research Grant Council (621709, 621011), HKUST grants SRFI11SC05 and RPC10SC11, and the Nanoscience and Nanotechnology Program at HKUST. We would like to thank G. A. Bird for helpful discussion about the sound propagation problem, and his great effort to set up more physical boundary treatment for the oscillating piston.

References

1 Wang Chang C. S., Uhlenbeck, G. E.: On the propagation of sound in monatomic gases. In: Boer, J. D. and Uhlenbeck, G. E. (eds.) Studies in Statistical Mechanics. 43-75. North Holland, Amsterdam (1970).
2 Pekeris, C. L., Alterman, Z., Finkelstein, L., et al.: Propagation of sound in a gas of rigid spheres. Physics of Fluids **5**, 1608–1610 (1962)
3 Sirovich, L., Thurber, J. K.: Propagation of forced sound waves in rarefied gasdynamics. The Journal of the Acoustical Society of America **37**, 329–339 (1965)
4 Buckner, J. K., Ferziger, J. H.: Linearized boundary value problem for a gas and sound propagation. Physics of Fluids **9**, 2315–2322 (1966)
5 Thomas, J. R., Siewert, C. E.: Sound-wave propagation in a rarefied gas. Transport Theory and Statistical Physics **8**, 219–240 (1979)
6 Loyalka, S. K., Cheng, T. C.: Sound-wave propagation in a rarefied gas. Physics of Fluids **22**, 830–836 (1979)
7 Hadjiconstantinou, N. G., Garcia, A. L.: Molecular simulations of sound wave propagation in simple gases. Physics of Fluids **13**, 1040–1046 (2001)
8 Huang, J. C., Xu, K., Yu, P.: A unified gas-kinetic scheme for continuum and rarefied flows II: multi-dimensional cases. Communications in Computational Physics **12**, 662–690 (2012)
9 Xu, K., Huang, J. C.: A unified gas-kinetic scheme for continuum and rarefied flows. Journal of Computational Physics **229**, 7747–7764 (2010)
10 Xu, K., Huang, J. C.: An improved unified gas-kinetic scheme and the study of shock structures. IMA Journal of Applied Mathematics **76**, 698–711 (2011)
11 Greenspan, M.: Propagation of sound in five monatomic gases. Journal of the Acoustical Society of America **28**, 644–648 (1956)
12 Meyer, E., Sessler, G.: Schallausbreitung in Gasen bei hohen Frequenzen und sehr niedrigen Drucken. Zeitschrift für Physik A Hadrons and Nuclei **149**, 15–39 (1957)
13 Garcia, R. D. M., Siewert, C. E.: The linearized Boltzmann equation: sound-wave propagation in a rarefied gas. Zeitschrift für angewandte Mathematik und Physik **57**, 94–122 (2005)
14 Struchtrup, H.: Resonance in rarefied gases. Continuum Mechanics and Thermodynamics, (2011) DOI: 10.1007/s00161-011-0202-0
15 Sharipov, F., Marques, W. J., Kremer, G. M.: Free molecular sound propagation. The Journal of the Acoustical **112**, 395–401 (2002)
16 Schotter, R.: Rarefied gas acoustics in the noble gases. Physics of Fluids **17**, 1163–1168 (1974)